Journal of Catalysis 257 (2008) 172–180

Contents lists available at ScienceDirect

Journal of Catalysis

www.elsevier.com/locate/jcat

Cu/SiO_2 catalysts prepared by the ammonia-evaporation method: Texture, structure, and catalytic performance in hydrogenation of dimethyl oxalate to ethylene glycol

Liang-Feng Chen [a], Ping-Jun Guo [a], Ming-Hua Qiao [a,*], Shi-Run Yan [a], He-Xing Li [b], Wei Shen [a], Hua-Long Xu [a,*], Kang-Nian Fan [a]

[a] Department of Chemistry and Shanghai Key Laboratory of Molecular Catalysis and Innovative Materials, Fudan University, Shanghai 200433, PR China
[b] Department of Chemistry, Shanghai Normal University, Shanghai 200234, PR China

ARTICLE INFO

Article history:
Received 7 February 2008
Revised 3 April 2008
Accepted 23 April 2008
Available online 27 May 2008

Keywords:
Cu/SiO_2
Ammonia-evaporation
Copper phyllosilicate
Dimethyl oxalate
Ethylene glycol
Hydrogenation

ABSTRACT

Cu/SiO_2 catalysts prepared by the ammonia-evaporation (AE) method have been systematically characterized focusing on the effect of the AE temperature during catalyst preparation. It is found that the texture, composition, and structure of the calcined and reduced Cu/SiO_2 catalysts were profoundly affected by the AE temperature. Based on characterizations and previous findings, the copper species on calcined Cu/SiO_2 samples and reduced Cu/SiO_2 catalysts were assigned. In gas-phase hydrogenation of dimethyl oxalate (DMO) to ethylene glycol (EG), the evolution of the catalytic activity with the Cu^0 and Cu^+ surface areas suggested that Cu^+ also participated in the hydrogenation process. The cooperative effect between Cu^0 and Cu^+ is proposed to be responsible for the highest hydrogenation activity of the Cu/SiO_2 catalyst prepared at the AE temperature of 363 K, on which an EG yield of 98% was obtained under the optimized hydrogenation conditions.

© 2008 Elsevier Inc. All rights reserved.

1. Introduction

Ethylene glycol (EG) is an important chemical widely used as antifreezer and in polyester manufacture [1]. At present, ethylene oxidation is a universal industrial approach to produce EG. However, as crude oil resource shrinks, synthesis of EG from syngas attracts more and more interest. This indirect synthesis process includes two steps: the coupling of CO with nitrite esters to oxalates, and the hydrogenation of oxalates to EG [2–7]. Considerable works have been devoted to the hydrogenation of oxalates since the 1970s. Matteoli et al. [8–13] have investigated the homogeneous hydrogenation of oxalates, and obtained an EG yield of 82% under H_2 pressure of 20 MPa at 453 K using $Ru(CO)_2(Ac)_2(PBu)_3$ as the catalyst. Recently, Teunissen and coworkers [14,15] applied Ru-based homogeneous catalysts in the hydrogenation of dimethyl oxalate (DMO); an EG yield of 95% was obtained under milder conditions (7 MPa, 373 K).

Being aware of the difficulties in the catalyst–product separation for the homogeneous catalysts, Cu-based heterogeneous catalysts have been investigated in the hydrogenation of dialkyl oxalates. Although on CuCr catalysts a high yield of EG was obtained [16–20], the toxicity of Cr severely limits its practical application. Therefore, Cr-free Cu-based catalysts supported on different carriers (SiO_2, Al_2O_3, ZnO, and La_2O_3) were studied [4,21–26], among which the Cu/SiO_2 catalyst afforded the highest yield of EG in the hydrogenation of DMO [25] and diethyl oxalate [4] due to the weak acidic and basic properties of SiO_2. It is known that strong acid sites induce the intermolecular dehydration of EG to ethanol, whereas strong basic sites catalyze the Guerbet reaction into the formation of 1,2-butanediol (1,2-BDO) [27,28], both of which deteriorate the selectivity to EG.

In above-mentioned works, the Cu/SiO_2 catalysts were mainly prepared by the homogeneous deposition–precipitation method, but the effect of the deposition–precipitation temperature remains to be explored. Van der Grift et al. [29] identified the formation of copper phyllosilicate on Cu/SiO_2 catalyst prepared by the homogeneous deposition–precipitation method. However, the influences of the deposition–precipitation temperature on the kinds of copper species formed and on the catalytic activity were not studied. It should be mentioned that for the Ni/SiO_2 catalyst prepared by the deposition–precipitation method, the preparation temperature and time determined the crystallinity and even the type of nickel phyllosilicate [30].

The present work was built on previous studies on the preparation of Cu/SiO_2 catalysts by the ammonia-evaporation (AE) method, a kind of the homogeneous deposition–precipitation method which

* Corresponding authors. Fax: +86 21 65641740.
E-mail addresses: mhqiao@fudan.edu.cn (M.-H. Qiao), shuhl@fudan.edu.cn (H.-L. Xu).

0021-9517/$ – see front matter © 2008 Elsevier Inc. All rights reserved.
doi:10.1016/j.jcat.2008.04.021

can conveniently and effectively disperse copper species on silica [21], with the added dimension of exploring the influences of the AE temperature on the texture and phase composition of the calcined Cu/SiO_2 samples. The catalytic performance of the reduced Cu/SiO_2 catalysts was evaluated using gas phase hydrogenation of DMO as the probe reaction. The nature of the active sites on the reduced Cu/SiO_2 catalysts was discussed and correlated with the characterization and activity results.

2. Experimental

2.1. Catalyst preparation

The Cu/SiO_2 catalysts were prepared by the AE method described as follows. 15.25 g of $Cu(NO_3)_2{\cdot}3H_2O$ (A.R., Sinopharm Chemical Reagent Ltd.) was dissolved in 150 ml of deionized water. 46 ml of 28% ammonia aqueous solution (A.R., Sinopharm Chemical Reagent Ltd.) was added and stirred for 30 min. Then 40.0 g of silica sol (Ludox AS-40) was added to the copper ammonia complex solution and stirred for another 4 h. The initial pH of the suspension was 11–12. All the above operations were performed at room temperature. The suspension was transferred to an oil bath preheated at 333, 343, 353, 363, and 373 K, respectively, to allow for the evaporation of ammonia and the decrease of pH and consequently, the deposition of copper species on silica. When the pH value of the suspension decreased to 6–7, the evaporation process was terminated. The filtrate was washed with 500 ml of deionized water five times and dried at 393 K overnight. The catalyst precursors were calcined in static air at 723 K for 4 h, pelletized, crushed, sieved to 40–60 meshes, and denoted as CuSiO-T, where T represents the AE temperature in Kelvin. The reduced catalysts were denoted as CuSi-T correspondingly.

2.2. Catalyst characterization

The bulk composition was analyzed by inductively coupled plasma-atomic emission spectroscopy (ICP-AES; IRIS Intrepid). The BET surface area (S_{BET}) was measured using N_2 physisorption at 77 K on a Micromeritics TriStar3000 apparatus. The X-ray diffraction (XRD) patterns were collected on a Bruker AXS D8 Advance X-ray diffractometer using Cu$K\alpha$ radiation ($\lambda = 0.15418$ nm). The tube voltage was 40 kV, and the current was 40 mA. For the reduced catalyst, Ar was used to protect the sample from oxidation during data acquisition.

IR spectra were recorded on a Nicolet Nexus 470 spectrometer equipped with a DTGS detector. The samples were finely grounded, dispersed in KBr, and pelletized. The spectral resolution was 2 cm^{-1}, and 32 scans were recorded for each spectrum. The particle size and distribution were observed by transmission electron microscopy (TEM; JEOL JEM2011). The surface species were detected by X-ray photoelectron spectroscopy (XPS; Perkin Elmer PHI5000C). The spectrum was recorded with Mg$K\alpha$ line as the excitation source ($h\nu = 1253.6$ eV). The binding energy (BE) values were referenced to the C 1s peak of contaminant carbon at 284.6 eV with an uncertainty of ±0.2 eV.

Temperature-programmed reduction (TPR) was carried out on a home-made apparatus. 20 mg of the calcined Cu/SiO_2 sample was outgassed at 473 K under Ar for 1 h. After cooling to room temperature under Ar, the gas was switched to 5% H_2/Ar, and the sample was heated to 723 K at a ramping rate of 10 K min^{-1}. The amount of H_2 consumed was monitored by a thermal conductivity detector (TCD). The metallic Cu surface area was measured by N_2O decomposition at 363 K using a pulsed method with N_2 as the carrier gas [31]. The consumption of N_2O was detected by a TCD. An adsorption stoichiometry of two Cu atoms per O atom and a Cu surface density of 1.46×10^{19} Cu atom m^{-2} were assumed.

2.3. Activity test and product analysis

The activity test was conducted on a continuous flow unit equipped with a stainless-steel fixed-bed tubular reactor. The catalyst bed had an inner diameter of 10 mm with a height of approximately 40 mm. Both sides of the catalyst bed were packed with quartz powders (20–40 meshes) to ensure a plug flow profile of the feed. The catalyst was activated in a 5% H_2/Ar atmosphere at 623 K for 4 h at a ramping rate of 2 K min^{-1}. After cooling to the reaction temperature of 473 K, 20 wt% DMO (purity >99%) in methanol and H_2 were fed into the reactor at a H_2/DMO molar ratio of 50 and a system pressure of 2.5 MPa. The room-temperature space velocity (LHSV) of DMO was varied from 0.10 to 0.50 h^{-1}. The products were condensed and analyzed by a gas chromatograph (Finnigan TraceGC ultra) fitted with a 30 m HP-5 capillary column and a flame ionization detector (FID).

3. Results

3.1. Characterization of calcined samples

3.1.1. Chemical composition and porosity

The Cu contents in the calcined Cu/SiO_2 samples are summarized in Table 1. The Cu contents are 14.7 and 15.7 wt% at AE temperatures of 333 and 343 K, respectively, which are lower than those at higher AE temperatures (~17.6 wt%). At low AE temperatures, the filtrate was deep blue-colored, indicating the incomplete precipitation of the Cu species.

The N_2 adsorption–desorption isotherms of the calcined Cu/SiO_2 samples and their pore size distribution curves are illustrated in Fig. 1. The BET surface area, pore volume, and average pore diameter are summarized in Table 1. It is found that the BET surface area increased from 156 to 326 $m^2\,g^{-1}$ when the AE temperature increased from 333 to 373 K. The pore shape of the calcined Cu/SiO_2 samples changed from "spherical" to "slit-like" with the increase of the AE temperature. The change was especially prominent when the samples prepared at 333 and 363 K were compared. The pore size distribution curves derived from the desorption branch using the BJH algorithm (Fig. 1B) show that at elevated AE temperatures, the contribution of pores at ca. 3.0 and 11.1 nm to the total pore volume increased considerably at the expense of pores at ca. 18.3 nm, which is consistent with the decrease of the average pore diameter from 11.6 to ca. 8.2 nm. It is noted that the pore volume and average pore diameter of the CuSiO-363 sample deviated from the trend displayed by other samples.

3.1.2. Crystalline phase and morphology

Fig. 2 shows the XRD patterns of the calcined Cu/SiO_2 samples, in which the feature at 2θ of around 22° came from amorphous silica. At the AE temperature of 333 K, the calcined Cu/SiO_2 sample exhibited diffractions characteristic of CuO (tenorite) at 2θ of 35.6 and 38.7° (JCPDS 05-0661), which were dramatically weakened at 343 K and finally vanished at elevated temperatures. The CuO crystallite sizes of the CuSiO-333 and CuSiO-343 samples are 11.7 and 10.1 nm, respectively, based on the Scherrer formula. Although the

Table 1
Physicochemical properties of the calcined Cu/SiO_2 samples

Sample	Cu loading (wt%)	S_{BET} ($m^2\,g^{-1}$)	V_p ($cm^3\,g^{-1}$)	d_p (nm)	d_{CuO}[a] (nm)
CuSiO-333	14.7	156	0.56	11.6	11.7
CuSiO-343	15.7	209	0.80	11.5	10.1
CuSiO-353	17.3	274	0.98	9.5	–
CuSiO-363	17.6	320	0.83	8.2	–
CuSiO-373	17.8	326	0.98	8.3	–

[a] CuO crystallite size calculated by the Scherrer formula.

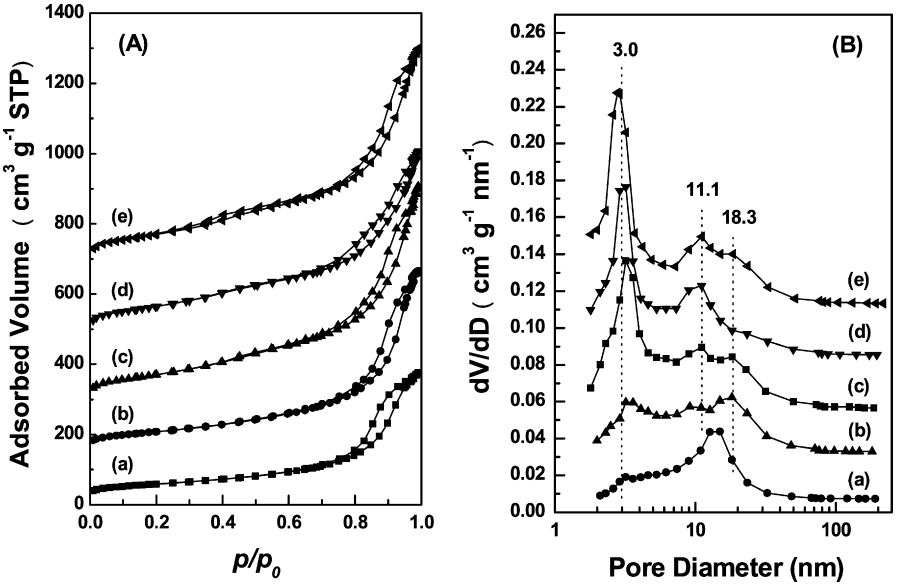

Fig. 1. N_2 adsorption–desorption isotherms (A) and pore size distribution curves calculated by BJH equation in desorption branch (B) of the calcined Cu/SiO_2 samples prepared at the AE temperature of (a) 333 K, (b) 343 K, (c) 353 K, (d) 363 K, and (e) 373 K.

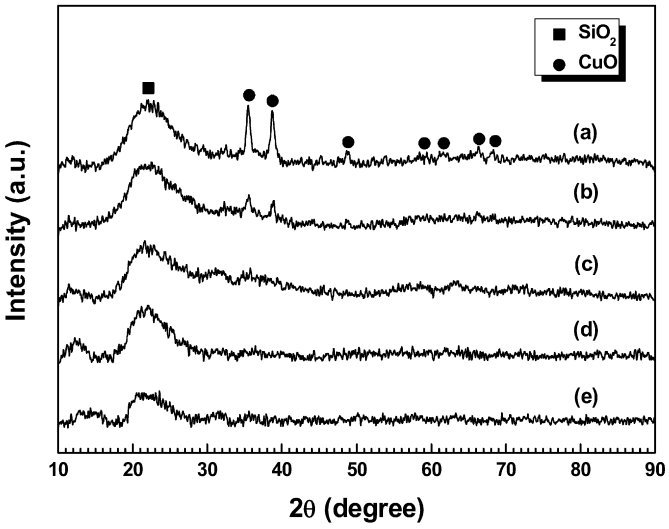

Fig. 2. XRD patterns of the calcined Cu/SiO_2 samples. (a) CuSiO-333, (b) CuSiO-343, (c) CuSiO-353, (d) CuSiO-363, and (e) CuSiO-373.

weak and broad diffraction peaks at ca. 31.2 and 35.8° suggest the presence of copper phyllosilicate with poor crystallinity [32], more unambiguous evidence supporting the formation of this phase is given below.

The disappearance of the CuO phase and the increased dispersion of copper species with the increase of the AE temperature can be directly observed in Fig. 3. In the TEM image of the calcined CuSiO-333 sample (Fig. 3a), light gray spherical silica particles are identified along with dark ones assignable to CuO. The latter reduced in amount at higher AE temperatures, suggesting the improved dispersion of CuO and/or the formation of phases other than CuO. For CuSiO-353, CuSiO-363, and CuSiO-373 samples, randomly oriented filandrous structure was observed, with the amount of the filandrous species in the CuSiO-363 sample being the most abundant.

IR technique has been adopted to determine the filandrous compounds of phyllosilicates [32–34]. In this work, as shown in Fig. 4, the formation of copper phyllosilicate is supported by the appearance of the δ_{OH} band at 663 cm^{-1} and the ν_{SiO} shoulder peak at 1040 cm^{-1} on the low frequency side of the ν_{SiO} asymmetric stretching band of SiO_2 at 1110 cm^{-1} [32]. The relative amount of copper phyllosilicate in calcined Cu/SiO_2 samples is calculated by considering the integrated intensity of the δ_{OH} band at 663 cm^{-1} normalized to the integrated intensity of the ν_{SiO} symmetric stretching band of SiO_2 at 800 cm^{-1}, which is termed as I_{663}/I_{800} [32]. It is worthwhile to note that the I_{663}/I_{800} ratio only gives a qualitative estimation of the amount of copper phyllosilicate, because the extinction coefficients of the corresponding IR bands are not known. Inset in Fig. 4 clearly shows that the relative amount of copper phyllosilicate in calcined Cu/SiO_2 samples increased with the AE temperature and maximized at 363 K.

3.1.3. Chemical state of copper and reduction behavior

XPS analysis was carried out to elucidate the chemical states of copper. Typically, the Cu $2p_{3/2}$ BE of CuO is found at ca. 933.5 eV [35], and the Cu $2p_{3/2}$ BE of supported copper phyllosilicate is 934.9 eV [29]. Fig. 5 shows that in all calcined Cu/SiO_2 samples copper existed in the oxidation state of Cu^{2+}, as evidenced by the Cu $2p_{3/2}$ peak at 933.1–935.6 eV and the $2p \rightarrow 3d$ satellite at 942–944 eV characteristic of Cu^{2+} with electron configuration of d^9 [36]. The variation of the Cu $2p_{3/2}$ BE values with the AE temperatures is an indication of the formation of different copper species in calcined Cu/SiO_2 samples.

Fig. 6 shows the TPR profiles of the calcined Cu/SiO_2 samples. For the CuSiO-333 sample, besides the main reduction peak at 516 K, there was a shoulder peak at ca. 540 K, which was attenuated for the CuSiO-343 sample, and vanished at higher AE temperatures. Based on the XRD and TEM characterizations, this shoulder peak is assigned to the reduction of large CuO particles to metallic Cu. The assignment is in compliance with the fact that the reduction of bulk CuO usually occurs at 528–573 K [37–39]. On the other hand, the main reduction peak at lower temperature is assigned to the reduction of other Cu species but not confined to copper phyllosilicate. A detailed assignment of the Cu species relating to the main reduction peak will be given in Section 4.3.

3.2. Characterization of the reduced catalysts

3.2.1. BET surface area and porosity

The N_2 adsorption–desorption isotherms of the reduced Cu/SiO_2 catalysts and their pore size distribution curves are plotted in

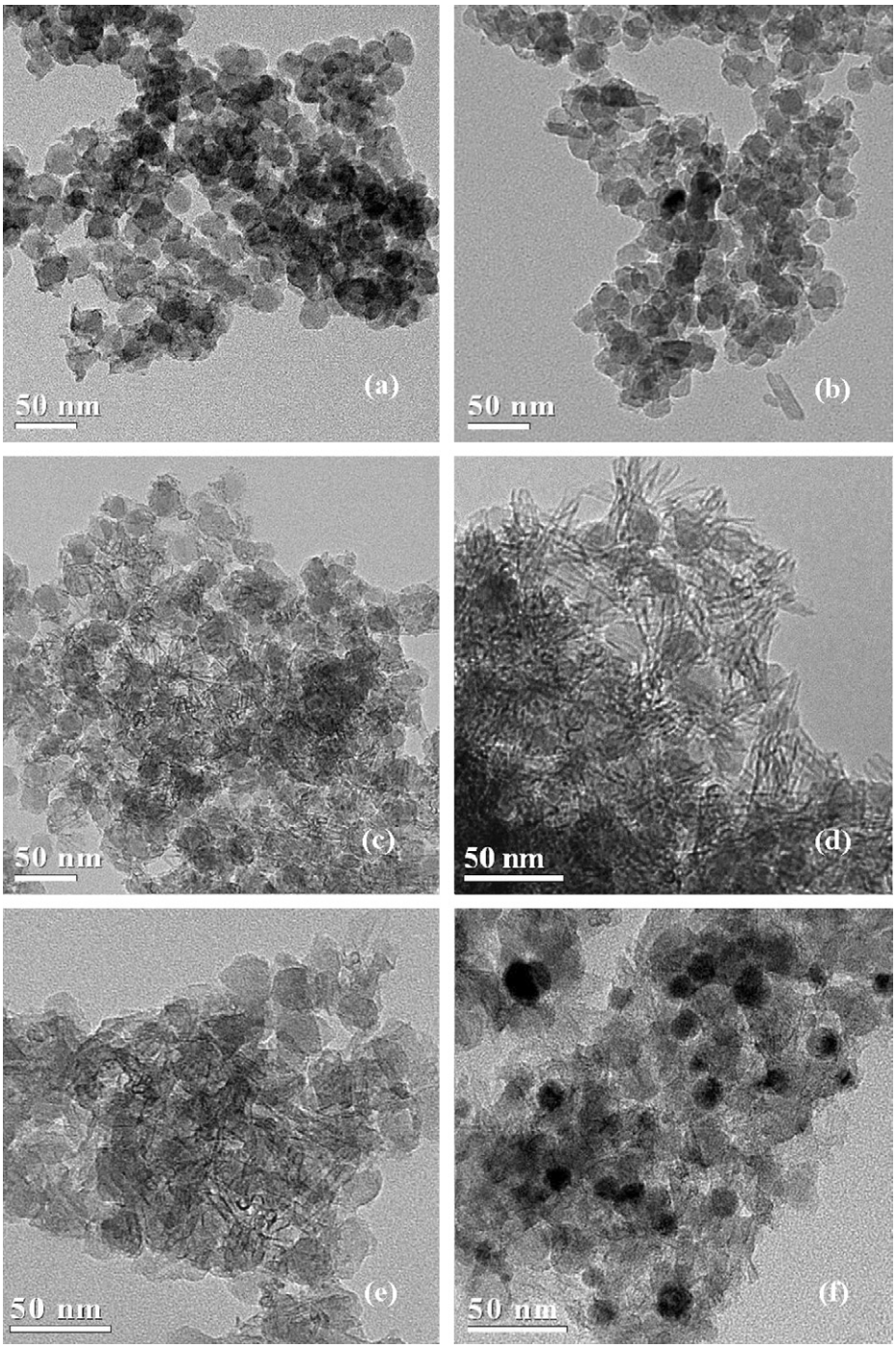

Fig. 3. TEM images of the calcined Cu/SiO_2 samples. (a) CuSiO-333, (b) CuSiO-343, (c) CuSiO-353, (d) CuSiO-363, and (e) CuSiO-373. (f) is the TEM image for the reduced CuSi-363 catalyst.

Fig. 7. The BET surface area, pore volume, and average pore diameter are summarized in Table 2. After reduction, the isotherms and pore size distribution curves still resembled those of calcined Cu/SiO_2 samples, except for the shift of the peak with the smallest pore size from ca. 3.0 to 2.4 nm and the decreased contribution of this peak to the total pore volume. As a result, the average pore diameter increased. In addition, the BET surface area and the total pore volume decreased, while their evolution with the AE temperature followed that of calcined Cu/SiO_2 samples. It is again noticed that similar to the CuSiO-363 sample, the CuSi-363 catalyst has pore volume and average pore diameter not in line with the trend held by other reduced catalysts.

3.2.2. Crystalline phase and morphology

The XRD patterns (Fig. 8) of the reduced Cu/SiO_2 catalysts show a strong diffraction peak at 2θ of 43.3° along with two weak ones at 50.4 and 74.1° characteristic of fcc Cu (JCPDS 04-0836). The Cu crystallite sizes calculated by the Scherrer formula are listed in Table 2. For the CuSi-333 catalyst, the Cu crystallite size showed a bimodal distribution at 5.2 and 22.1 nm, which was also observed but not as obvious for the CuSi-343 catalyst, as identified by fitting the Cu(111) diffraction peak at 43.3°. The bimodal distribution of the Cu particle size for the CuSi-333 and CuSi-343 catalysts is visible by TEM as well, as listed in Table 2. On other reduced Cu/SiO_2 catalysts, only Cu crystallites with size of ca. 4 nm were identified.

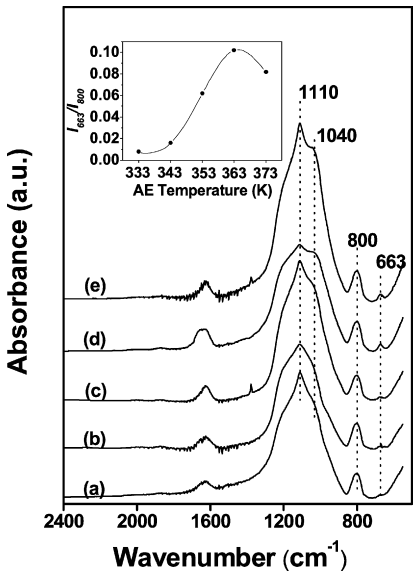

Fig. 4. IR spectra of the calcined Cu/SiO_2 samples. (a) CuSiO-333, (b) CuSiO-343, (c) CuSiO-353, (d) CuSiO-363, and (e) CuSiO-373. Inset shows the I_{663}/I_{800} intensity ratio representing the relative amount of copper phyllosilicate in the precursors.

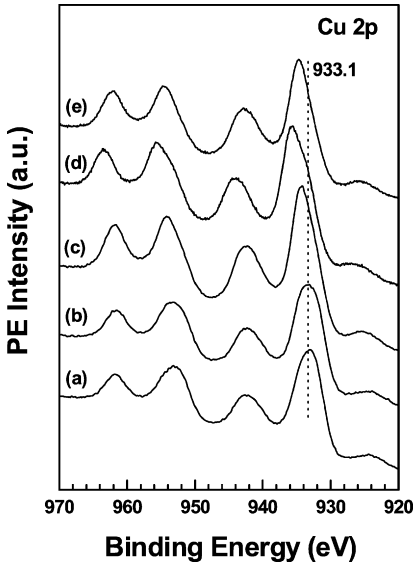

Fig. 5. XPS spectra of the calcined Cu/SiO_2 samples. (a) CuSiO-333, (b) CuSiO-343, (c) CuSiO-353, (d) CuSiO-363, and (e) CuSiO-373.

In addition, all reduced catalysts showed a weak and broad peak at around 36.4° ascribable to the $Cu_2O(111)$ plane (JCPDS 05-0667), indicating that a portion of copper exists as Cu^+ after reduction in H_2 at 623 K. Among the reduced Cu/SiO_2 catalysts, the CuSi-363 catalyst showed the most distinct Cu_2O (111) diffraction peak.

The TEM image of the CuSi-363 catalyst is shown in Fig. 3f as an example for the reduced Cu/SiO_2 catalysts. A comparison with the TEM image of the CuSiO-363 sample (Fig. 3d) clearly demonstrates that after reduction the typical filandrous morphology of copper phyllosilicate was eliminated substantially, whereas black spherical particles attributable to metallic Cu emerged. The metallic Cu particle size observed by TEM is larger than the crystallite size derived from XRD, indicating the polycrystalline nature of the metallic Cu particles.

3.2.3. Surface chemical states

The XPS and X-ray induced Auger spectra (XAES) of the reduced Cu/SiO_2 catalysts are illustrated in Figs. 9 and 10, respectively. As

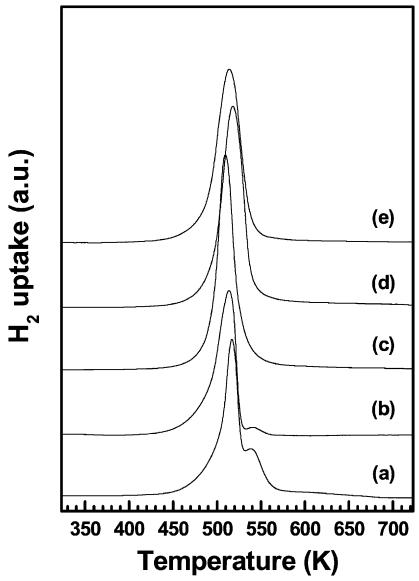

Fig. 6. H_2-TPR profiles of the calcined Cu/SiO_2 samples. (a) CuSiO-333, (b) CuSiO-343, (c) CuSiO-353, (d) CuSiO-363, and (e) CuSiO-373.

Table 2
Physicochemical properties of the reduced Cu/SiO_2 catalysts

Catalyst	S_{BET} ($m^2\,g^{-1}$)	V_p ($cm^3\,g^{-1}$)	d_p (nm)	d_{Cu}[a] (nm)	d_{Cu}[c] (nm)
CuSi-333	132	0.50	14.0	22.1, 5.2[b]	30.2, 6.4
CuSi-343	181	0.75	13.5	15.7, 4.8[b]	14.3, 6.1
CuSi-353	248	0.77	12.3	4.1	7.1
CuSi-363	281	0.71	9.0	3.6	7.3
CuSi-373	309	0.96	10.3	3.9	7.2

[a] Cu crystallite size calculated by the Scherrer formula.
[b] Bimodal size distribution of Cu crystallites calculated by fitting the (111) diffraction peak of fcc Cu.
[c] Cu particle size measured by TEM.

compared to the calcined samples, the Cu $2p_{3/2}$ BE of the reduced catalysts shifted to ca. 932.7 eV, and the $2p \rightarrow 3d$ satellite disappeared due to the reduction of Cu^{2+} to Cu^0 or/and Cu^+. The modified Auger parameter α', which represents the summation of the kinetic energy (KE) of the Cu LMM Auger electron and the BE of the Cu $2p_{3/2}$ photoelectron, was employed to distinguish between the Cu^0 and Cu^+ species. In general, α' is ca. 1851.0 eV for Cu^0 and 1849.0 eV for Cu^+ [40]. In Fig. 10, it is obvious that each Cu LMM spectrum contains one more component as inferred by the broad and asymmetrical peak shape; the deconvolution results are listed in Table 3. The α' value at ca. 1851.0 eV is ascribed to Cu^0 and ca. 1847.0 eV to Cu^+. The smaller α' value for Cu^+ than the bulk value is attributed to the strong interaction between Cu^+ and SiO_2. It is reported that when copper (in +2, +1, and 0 valence) is in the highly dispersed state and in intimate contact with the supports, α' can be 2–3 eV lower than the bulk values [41].

As listed in Table 3, the $Cu^+/(Cu^+ + Cu^0)$ intensity ratio derived by fitting the Cu LMM peak increased with the AE temperature, and maximized at 363 K with the $Cu^+/(Cu^+ + Cu^0)$ ratio of 54.9%. It has been shown that CuO species weakly interacting with the support can be readily reduced to Cu^0 at 623 K [42,43]. The high $Cu^+/(Cu^+ + Cu^0)$ ratios (>40%) for the reduced Cu/SiO_2 catalysts signify the hindrance for Cu^{2+} reduction in calcined Cu/SiO_2 samples prepared by the AE method.

The metallic Cu surface areas measured by N_2O titration are listed in Table 3. The Cu^0 surface area increased from 3.6 to 9.8 $m^2\,g^{-1}$ as the AE temperature increased, with the exception of the CuSi-363 catalyst having a Cu^0 surface area of 9.2 $m^2\,g^{-1}$,

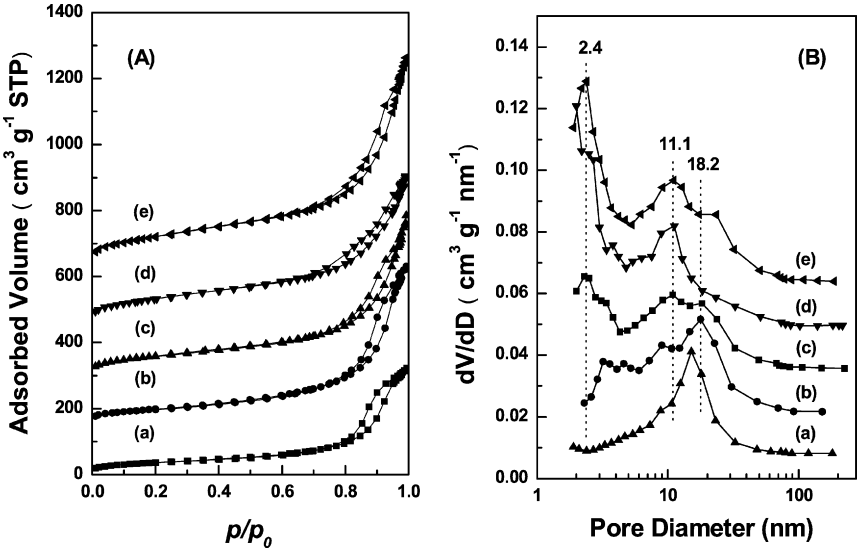

Fig. 7. N_2 adsorption–desorption isotherms (A) and pore size distribution curves calculated by BJH equation in desorption branch (B) of the reduced Cu/SiO_2 catalysts prepared at the AE temperature of (a) 333 K, (b) 343 K, (c) 353 K, (d) 363 K, and (e) 373 K.

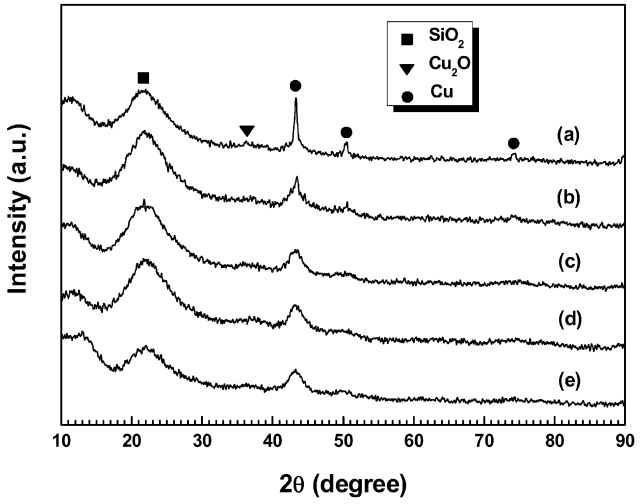

Fig. 8. XRD patterns of the reduced Cu/SiO_2 catalysts. (a) CuSi-333, (b) CuSi-343, (c) CuSi-353, (d) CuSi-363, and (e) CuSi-373.

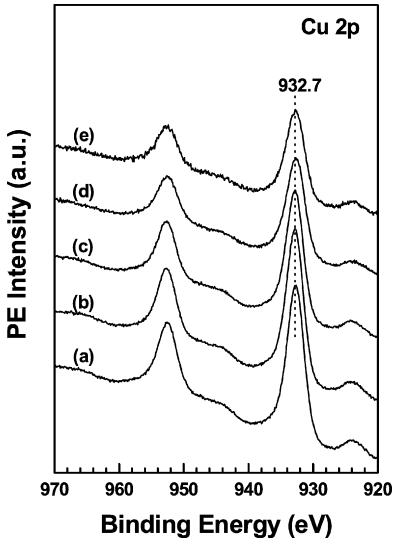

Fig. 9. XPS spectra of the reduced Cu/SiO_2 catalysts. (a) CuSi-333, (b) CuSi-343, (c) CuSi-353, (d) CuSi-363, and (e) CuSi-373.

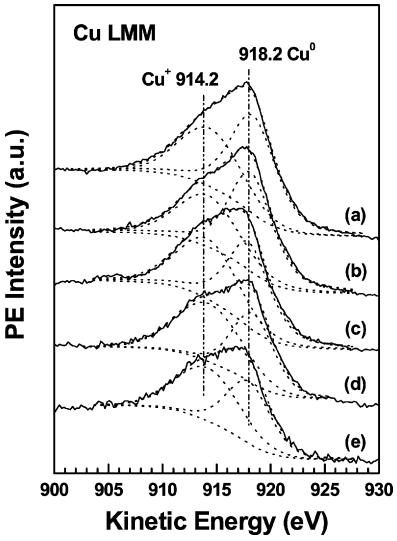

Fig. 10. Cu LMM Auger spectra of the reduced Cu/SiO_2 catalysts. (a) CuSi-333, (b) CuSi-343, (c) CuSi-353, (d) CuSi-363, and (e) CuSi-373. The Auger features due to Cu^0 and Cu^+ are indicated.

Table 3
Cu species on the reduced Cu/SiO_2 catalyst derived from Cu LMM XAES spectra

Catalyst	KE (eV)		α' (eV)		X_{Cu^+} [a] (%)	S_{Cu^0} [b] ($m^2\,g^{-1}$)	S_{Cu^+} [c] ($m^2\,g^{-1}$)
	Cu^+	Cu^0	Cu^+	Cu^0			
CuSi-333	914.4	918.4	1847.0	1851.0	40.4	3.6	2.4
CuSi-343	914.2	918.2	1847.0	1851.0	40.5	7.8	5.3
CuSi-353	914.2	918.0	1846.9	1850.7	45.7	9.6	8.1
CuSi-363	914.3	918.4	1846.9	1851.0	54.9	9.2	11.2
CuSi-373	914.2	918.0	1846.8	1850.6	52.0	9.8	10.6

[a] Intensity ratio between Cu^+ and ($Cu^+ + Cu^0$) by deconvolution of Cu LMM XAES spectra.

[b] Metallic Cu surface area determined by N_2O titration.

[c] Calculated based on X_{Cu^+} and S_{Cu^0} assuming that Cu^+ ion occupies the same area as that of the Cu^0 atom, and has the same atomic sensitivity factor as that of Cu^0.

which is smaller than its neighboring catalysts. As revealed by the Cu LMM XAES results, the Cu species on the reduced Cu/SiO_2 catalysts are Cu^0 and Cu^+. Assuming that the Cu^+ ion occupies the same area as that of the Cu^0 atom, and has the same atomic sen-

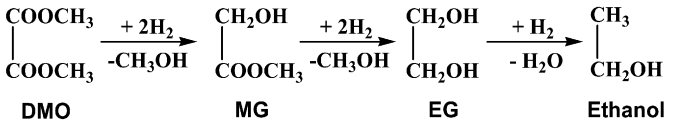

Scheme 1. Reaction pathway for the hydrogenation of DMO to MG, EG, and ethanol.

Table 4
The catalytic performance of the Cu/SiO_2 catalysts prepared by the AE method in gas-phase hydrogenation of DMO[a]

Catalyst	DMO conversion (%)	Selectivity (%)			
		MG	EG	Ethanol	1,2-BDO
CuSi-333	34	82	18	0.7	0.2
CuSi-343	46	73	26	1.5	0
CuSi-353	65	65	33	1.7	0
CuSi-363	79	57	43	1.8	0
CuSi-373	73	74	25	1.1	0.1

[a] Reaction conditions: $p = 2.5$ MPa, $T = 473$ K, H_2/DMO = 50 (mol mol^{-1}), and LHSV of DMO = 0.50 h^{-1}.

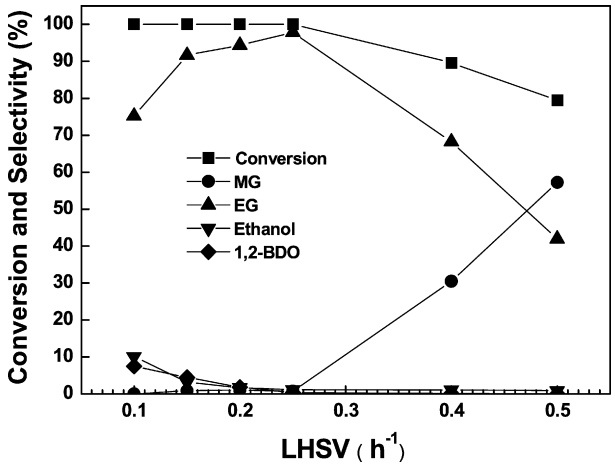

Fig. 11. Effect of the LHSV of DMO on the catalytic performance of the CuSi-363 catalyst. Reaction conditions: $p = 2.5$ MPa, $T = 473$ K, and H_2/DMM = 50 (mol mol^{-1}).

sitivity factor as that of Cu^0, the Cu^+ surface area was estimated according to the Cu^0 surface area and the surface $Cu^+/(Cu^+ + Cu^0)$ LMM intensity ratio. In Table 3, it is found that different from the evolution of the Cu^0 surface area, the Cu^+ surface area maximized at the AE temperature of 363 K, with the value of 11.2 m^2 g^{-1}.

3.3. Gas-phase hydrogenation of DMO

The catalytic performance of the Cu/SiO_2 catalysts prepared at different AE temperatures was investigated in gas-phase hydrogenation of DMO. Steady-state product compositions were obtained after about 8 h on stream. It is known that the hydrogenation of DMO proceeds via methyl glycolate (MG) to EG, while EG can dehydrate further to ethanol (Scheme 1). The reaction between EG and ethanol on basic sites yields 1,2-BDO [28]. Under the reaction condition specified under Table 4, the conversion of DMO increased steadily from 34% on the CuSi-333 catalyst to 79% on the CuSi-363 catalyst, and then dropped to 73% on the CuSi-373 catalyst. Almost all the converted DMO had been turned into MG and EG. The selectivities to ethanol and 1,2-BDO remained low (<2%), attributable to the lacking of acid and basic sites on SiO_2.

Over the CuSi-363 catalyst which exhibited the highest hydrogenation activity, while keeping other reaction conditions unchanged, the LHSV of DMO was adjusted to optimize the yield of EG. In Fig. 11, the conversion of DMO and selectivities to ethanol and 1,2-BDO decreased with the increase of LHSV, whereas the selectivity to MG increased only slightly below LHSV of 0.25 h^{-1}, then grew up drastically. As a result, the EG selectivity reached a maximum of 98% at the LHSV of 0.25 h^{-1} when the DMO conversion still remained at about 100%.

4. Discussion

4.1. Formation of copper phyllosilicate on calcined Cu/SiO_2 samples

Copper phyllosilicate ($Cu_2Si_2O_5(OH)_2$), also called chrysocolla, is a kind of copper silicate with lamellar structure that consists of layers of SiO_4 tetrahedra sandwiched between discontinuous layers of CuO_6 octahedra. Copper phyllosilicate is known to form during the preparation of Cu/SiO_2 catalyst by the deposition–precipitation method using urea hydrolysis [29] and by selective adsorption of $Cu(NH_3)_4^{2+}$ on SiO_2 [32]. Our work showed that copper phyllosilicate can also be formed using the AE method. Van der Grift et al. [29] reported that the BET surface area of the Cu/SiO_2 catalyst prepared by the urea hydrolysis method increased with the increase of the Cu loading, and ascribed it to the formation of more filandrous copper phyllosilicate which enhanced the BET surface area. In the present work, the BET surface areas of the calcined Cu/SiO_2 samples increased with the AE temperature. The formation of copper phyllosilicate is also corroborated by IR. TEM images showed that the filandrous structure characteristic of copper phyllosilicate became predominant on samples with higher AE temperatures. Therefore, the change in the pore shape from "spherical" to "slit-like" and the decrease in the average pore size can be attributed to the formation of a new pore system arising from the filandrous copper phyllosilicate.

For both the calcined Cu/SiO_2 samples and the reduced Cu/SiO_2 catalysts, N_2 physisorption, TEM, IR, XPS, and TPR characterizations all point to the similar character of the samples prepared at AE temperatures of 353 and 373 K. As reported by Burattin et al. [30], the formation of nickel phyllosilicate during deposition–precipitation by urea hydrolysis was facilitated by longer preparation time and higher temperature. In the present case, although the preparation method and the formed phyllosilicate are different, the synthesis time may also play an important role in the formation of copper phyllosilicate. But for the AE method used here, a higher preparation temperature means more rapid evaporation of ammonia, thus a shorter time for the pH of the suspension decreasing from 11–12 to 6–7. The similarity between calcined Cu/SiO_2 samples prepared at AE temperatures of 353 and 373 K can be rationalized in terms of the interplay between the AE temperature and the AE time. At the optimal AE temperature, 363 K, the amount of copper phyllosilicate became the most abundant, as supported by TEM and IR results shown in Figs. 3 and 4, respectively.

4.2. Copper species on calcined Cu/SiO_2 samples prepared by the AE method

The ion-exchange method reported by Kobayashi et al. [44] and Kohler et al. [41] resembles to some extent with the AE method used here. For both methods, SiO_2 was immersed in the $Cu(NH_3)_4^{2+}$ solution at the pH value of 11–12 at room temperature until adsorption and ion-exchange reached a dynamic equilibrium. The difference is that evaporation of ammonia instead of filtration was followed in the AE method. The Cu species on the calcined Cu/SiO_2 catalyst prepared by the ion-exchange method are present in two forms. One is the immobilized single Cu ions on SiO_2 surface by exchanging with two silanol group, the other is a well dispersed CuO layer over the ion-exchanged Cu–O–Si layer, which originates from the calcination of $Cu(OH)_2$ formed during washing by water that hydrolyzes $Cu(NH_3)_4^{2+}$ trapped in the filter cake [41]. Using

the AE method, $Cu(OH)_2$ may analogously form, because the evaporation of ammonia also led to the decrement of the pH of the suspension. Thus we suggest that on calcined Cu/SiO_2 samples prepared at low AE temperatures, besides the presence of a small amount of large CuO particles (~10 nm) identified by XRD, TEM, and H_2-TPR, there are ion-exchanged Cu–O–Si layer and well dispersed CuO over the ion-exchanged layer. The formation of large CuO particles is attributed to the aggregation of some loosely-bonding well dispersed CuO during calcination.

On the other hand, van der Grift et al. [45] found that a fraction of copper phyllosilicate undergoes decomposition during calcination, resulting in well dispersed CuO accompanied by the intact copper phyllosilicate. The extent of decomposition depends on the preparation conditions and the thermal pretreatment of copper phyllosilicate. Toupance et al. also revealed a partial decomposition of copper phyllosilicate when being calcined at 723 K [46]. Therefore, aside from copper phyllosilicate identified by TEM and IR, there should be another kind of well dispersed CuO on calcined Cu/SiO_2 samples prepared at high AE temperatures due to partial decomposition of copper phyllosilicate during calcination at 723 K for 4 h. The coexistence of the well dispersed CuO with copper phyllosilicate can explain the asymmetric line-shape of the Cu $2p_{3/2}$ peaks of the CuSiO-353, CuSiO-363, and CuSiO-373 samples in Fig. 5.

In brief, on CuSiO-333 and CuSiO-343 samples, there are three kinds of copper species: ion-exchanged Cu–O–Si layer, well dispersed CuO over the ion-exchanged layer, and a small amount of large CuO particles. On CuSiO-353, CuSiO-363, and CuSiO-373 samples, there are two kinds of copper species: copper phyllosilicate and another well dispersed CuO originating from the partial decomposition of copper phyllosilicate during calcination. Such assignments are validated further in the following section.

4.3. Copper species on the reduced Cu/SiO_2 catalysts prepared by the AE method

Although the well dispersed CuO species formed on calcined Cu/SiO_2 samples prepared at low and high AE temperatures have different origin, it is reasonable to assume that their reducibility is similar. For well dispersed CuO on ion-exchanged Cu/SiO_2 samples, the reduction temperature is 523 K, which is lower than that of bulk CuO [37]. On the $Cu/t\text{-}ZrO_2$ sample, the highly dispersed CuO is also reduced more facilely than large CuO particles [42]. The main reduction peak at ca. 520 K in Fig. 6 then can be partly attributed to the reduction of the well dispersed CuO species which led to small Cu crystallites of 3–5 nm on all the reduced Cu/SiO_2 catalysts (Table 2). Both Kohler et al. [41] and Toupance et al. [46] reported that the reduction of CuO/SiO_2 prepared by the ion-exchange method can result in small Cu crystallite size. Accordingly, the bimodal distribution of the Cu crystallite size on the CuSi-333 and CuSi-343 catalysts is interpreted as the reduction of large CuO particles at ca. 540 K and the reduction of the well dispersed CuO over the ion-exchanged Cu–O–Si layer at ca. 520 K.

For the ion-exchanged Cu–O–Si species and copper phyllosilicate, the reduction is ceased at Cu^+ under the present reduction condition due to the strong interaction between copper ions and SiO_2. Further reduction of Cu^+ to Cu^0 requires a temperature >873 K [37,45]. Marchi et al. [37] identified that the reduction of the ion-exchanged Cu–O–Si species to Cu^+ occurred at 523 K, which overlapped with the reduction peak of the well dispersed CuO to Cu^0. For calcined copper phyllosilicate, van der Grift et al. [47] identified only one reduction peak at ca. 510 K, suggesting the identical reduction temperature for copper phyllosilicate to Cu^+ and for the well dispersed CuO to Cu^0. The lower heating rate (3.4 $K\,min^{-1}$) used in that work is responsible for the slightly lower reduction temperature than ours (ca. 520 K). Thus, the strong reduction peak in Fig. 6 is attributed to the collective contribution of the reduction of the well dispersed CuO to Cu^0 and the ion-exchanged Cu–O–Si and copper phyllosilicate to Cu^+.

4.4. Active sites on the reduced Cu/SiO_2 catalysts for DMO hydrogenation

Although the Cu 2p spectra show that Cu^{2+} has been completely depleted after reduction, the broad and asymmetric peak shape of the Cu LMM Auger spectra indicate that Cu existed in one more chemical state on reduced Cu/SiO_2 catalysts. Deconvolution of Fig. 10 reveals that the reduced catalysts have a surface $Cu^+/(Cu^+ + Cu^0)$ intensity ratio >40%, attributable to the hindered reduction of Cu^{2+} in ion-exchanged Cu–O–Si species and copper phyllosilicate. It is notable that the CuSi-363 catalyst has the highest $Cu^+/(Cu^+ + Cu^0)$ ratio and the largest Cu^+ surface area, corresponding well to the largest amount of copper phyllosilicate in the calcined Cu/SiO_2 sample prepared at the AE temperature of 363 K.

In Table 4, the conversion of DMO is found to increase steadily on Cu/SiO_2 catalysts prepared at low AE temperatures, maximized on the CuSi-363 catalyst, and dropped on the CuSi-373 catalyst. Although lower Cu^0 surface area corresponded to lower conversion of DMO, at higher Cu^0 surface area, the correlation of the Cu^+ surface area with the catalytic activity became more apparent, implying that Cu^+ also played an indispensable role in hydrogenating DMO. It has been suggested that only Cu^0 acts as the active site in ester hydrogenation [48], but in methyl acetate hydrogenation Poels and Brands [49] reported that while Cu^0 dissociatively adsorbs H_2, Cu^+ stabilizes the methoxy and the acyl species which are also important intermediates in DMO hydrogenation. Moreover, Cu^+ may function as electrophilic or Lewis acid sites to polarize the C=O bond via the electron lone pair on oxygen [50], thus improving the reactivity of the ester group in DMO. So we tentatively propose that the optimal catalytic activity on the CuSi-363 catalyst lies in the cooperative effect between Cu^0 and Cu^+ to dissociate hydrogen and to activate DMO, respectively. Although using the ion-exchange method one can also obtain Cu/SiO_2 catalysts with the coexistence of the Cu^0 and Cu^+ species, the loading of Cu is low due to the intrinsic limitation of the method. The AE method then offers an effective way to prepare Cu/SiO_2 catalyst with higher loading of Cu^0 and Cu^+, which may be important for catalytic reactions such as DMO hydrogenation exemplified here, or for apparatus that have severe space limitations.

5. Conclusion

The present work demonstrated that the evaporation temperature of ammonia in the AE method has profound effects on the texture, composition, and structure of the calcined Cu/SiO_2 samples and reduced Cu/SiO_2 catalysts. The copper species on the calcined and reduced Cu/SiO_2 catalysts prepared at different AE temperatures were assigned based on characterizations and literature works. In gas-phase hydrogenation of DMO to EG, the evolution of the catalytic activity with the Cu^0 and Cu^+ surface areas suggests the cooperative effect between Cu^0 and Cu^+ which dissociates hydrogen and activates DMO, respectively. On the Cu/SiO_2 catalyst prepared at the AE temperature of 363 K, an EG yield of 98% was obtained under the optimized hydrogenation conditions.

Acknowledgments

This work was supported by the National Basic Research Program of China (2006CB202502), Shanghai Science and Technology Committee (06JC14009), the Fok Ying Tong Education Foundation (104022), and the NSF of China (20673025).

References

[1] G.H. Xu, Y.C. Li, Z.H. Li, H.J. Wang, Ind. Eng. Chem. Res. 34 (1995) 2371.
[2] L.R. Zehner, US4005131 (1977).
[3] M. Mitsunobu, F. Kouzou, N. Keigo, M. Masaoki, S. Hiroyuki, JP54103817 (1979).
[4] H. Miyazaki, T. Uda, K. Hirai, Y. Nakamura, H. Ikezawa, T. Tsuchie, US4585890 (1986).
[5] G.S. Chen, B. Xue, H.M. Yan, Chin. J. Catal. 13 (1992) 291.
[6] X.G. Zhao, X.L. Lv, H.G. Zhao, Y.Q. Zhu, W.D. Xiao, Chin. J. Catal. 27 (2004) 125.
[7] W.J. Bartley, W.V. Charleston, US4677234 (1987).
[8] U. Matteoli, G. Menchi, M. Bianchi, F. Piacenti, J. Organomet. Chem. 299 (1986) 233.
[9] U. Matteoli, M. Bianchi, G. Menchi, P. Frediani, F. Piacenti, J. Mol. Catal. 22 (1984) 353.
[10] U. Matteoli, M. Bianchi, G. Menchi, P. Frediani, F. Piacenti, J. Mol. Catal. 29 (1985) 269.
[11] U. Matteoli, G. Menchi, M. Bianchi, F. Piacenti, J. Mol. Catal. 44 (1988) 347.
[12] U. Matteoli, G. Menchi, M. Bianchi, F. Piacenti, J. Mol. Catal. 64 (1991) 257.
[13] U. Matteoli, G. Menchi, M. Bianchi, F. Piacenti, S. Ianelli, M. Nardelli, J. Organomet. Chem. 498 (1995) 177.
[14] H.T. Teunissen, C.J. Elsevier, Chem. Commun. (1997) 667.
[15] M.C. van Engelen, H.T. Teunissen, J.G. de Vries, C.J. Elsevier, J. Mol. Catal. A 206 (2003) 185.
[16] T. Susumu, F. Kozo, N. Keigo, M. Masaoki, M. Katsuhiko, EP0046983 (1982).
[17] M. Haruhiko, H. Kouichi, U. Taizou, N. Yasuo, I. Seizou, T. Takanori, JP57123127 (1982).
[18] P. Fedor, EP0060787 (1982).
[19] L.R. Zehner, R.W. Lenton, US4112245 (1978).
[20] D.M. Huang, Z.M. Chen, F.X. Chen, P. Lin, H.S. Lan, Y.F. He, Ind. Catal. 4 (1996) 24, (in Chinese).
[21] M. Haruhiko, H. Kouichi, U. Taizou, N. Yasuo, I. Seizou, T. Takanori, JP57122946 (1982).
[22] M. Haruhiko, H. Kouichi, U. Taizou, N. Yasuo, I. Seizou, T. Takanori, JP57122941 (1982).
[23] M. Haruhiko, H. Kouichi, U. Taizou, N. Yasuo, I. Seizou, T. Takanori, JP57122938 (1982).
[24] M. Haruhiko, H. Kouichi, U. Taizou, N. Yasuo, I. Seizou, T. Takanori, JP57122939 (1982).
[25] H. Kouichi, U. Taizou, N. Yasuo, US4614728 (1986).
[26] Z.X. Li, Ph.D. dissertation, East China University of Science and Technology (2006).
[27] P.B. Guan, The Manufacture and Application of Fatty Alcohols, Beijing Light Industry Press, Beijing, 1990, pp. 226–228.
[28] C. Carlini, M.D. Girolamo, A. Macinai, J. Mol. Catal. A 200 (2003) 137.
[29] C.J.G. van der Grift, P.A. Elberse, A. Mulder, J.W. Geus, Appl. Catal. 59 (1990) 275.
[30] P. Burattin, M. Che, C. Louis, J. Phys. Chem. B 101 (1997) 7060.
[31] J.W. Evans, M.S. Wainwright, A.J. Bridgewater, D.J. Young, Appl. Catal. 7 (1983) 75.
[32] T. Toupance, M. Kermmarec, J.F. Lambert, C. Louis, J. Phys. Chem. B 106 (2002) 2277.
[33] M. Kermarec, J.Y. Carriat, P. Burattin, M. Che, A. Decarreau, J. Phys. Chem. 98 (1994) 12008.
[34] O. Clause, M. Kermarec, L. Bonneviot, F. Villain, M. Che, J. Am. Chem. Soc. 114 (1992) 4709.
[35] A. Gervasini, M. Manzoli, G. Martra, A. Ponti, N. Ravasio, L. Sordelli, F. Zaccheria, J. Phys. Chem. B 110 (2006) 7851.
[36] F. Raimondi, K. Geissler, J. Wambach, A. Wokaun, Appl. Surf. Sci. 189 (2002) 59.
[37] A.J. Marchi, J.L.G. Fierro, J. Santamaría, A. Mozón, Appl. Catal. A 142 (1996) 375.
[38] M. Shimokawabe, N. Takezawa, H. Kobayashi, Appl. Catal. 2 (1982) 379.
[39] F.W. Chang, H.C. Yang, L.S. Roselin, W.Y. Kuo, Appl. Catal. A 304 (2006) 30.
[40] K.P. Sun, W.W. Lu, F.Y. Qiu, S.W. Liu, X.L. Xu, Appl. Catal. A 252 (2003) 243.
[41] M.A. Kohler, H.E. Curry-Hyde, A.E. Hughes, B.A. Sexton, N.W. Cant, J. Catal. 108 (1987) 323.
[42] Z. Liu, M.D. Amiridis, Y. Chen, J. Phys. Chem. B 109 (2005) 1251.
[43] E.L. Rodrigues, A.J. Marchi, C.R. Apesteguia, J.M.C. Bueno, Appl. Catal. A 294 (2005) 197.
[44] H. Kobayashi, N. Takezawa, C. Minochi, K. Takahashi, Chem. Lett. (1980) 1197.
[45] C.J.G. van der Grift, A.F.H. Wielers, A. Mulder, J.W. Geus, Thermochim. Acta 171 (1990) 95.
[46] T. Toupance, M. Kermarec, C. Louis, J. Phys. Chem. B 104 (2000) 965.
[47] C.J.G. van der Grift, A. Mulder, J.W. Geus, Appl. Catal. 60 (1990) 181.
[48] M. Mokhtar, C. Ohlinger, J.H. Schlander, T. Turek, Chem. Eng. Technol. 24 (2001) 423.
[49] E.K. Poels, D.S. Brands, Appl. Catal. A 191 (2000) 83.
[50] M. Bartók, Á. Molnár, in: S. Patai (Ed.), The Chemistry of Double-Bonded Functional Groups (Suppl. A3), Wiley, New York, 1997, chap. 16.